Vacuum 184 (2021) 109783

Contents lists available at ScienceDirect

Vacuum

journal homepage: http://www.elsevier.com/locate/vacuum

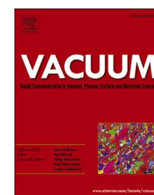

Non-treated low temperature indium tin oxide fabricated in oxygen-free environment to low-cost silicon-based solar technology

S. Fernández [a,*], J.P. González [a], J. Grandal [b], A.F. Braña [c], F. García [d], F. Borlaf [d], M. B. Gómez-Mancebo [d]

[a] Departamento de Energía, CIEMAT, Avda. Complutense 40, 28040, Madrid, Spain
[b] ISOM and E Universidad Politécnica de Madrid. Avda. Complutense 30, 28040, Madrid, Spain
[c] Grupo de Electronica y Semiconductores, Universidad Autónoma de Madrid, Avda. Francisco Tomás y Valiente 7, 28049, Madrid, Spain
[d] División de Química, CIEMAT, Avda. Complutense 40, 28040, Madrid, Spain

ARTICLE INFO

Keywords:
ITO
Amorphous materials
Magnetron sputtering
Silicon based solar cells

ABSTRACT

80 nm nominal thick ITO thin films were deposited at room temperature and at low plasma irradiation conditions in an oxygen-free environment by magnetron sputtering. The assessment of the dependence of their structural and optoelectronic properties with the deposition parameters were determined to evaluate their potential in silicon-based solar technology. The results revealed high quality ITO thin films deposited at room temperature and at low direct-current power values up to 75 W. These films showed amorphous and polycrystalline nature, depending on the range of power used. The thin films performance was determined by the figure of merit, reaching the best material developed at room temperature and at 75 W. The successful use of ITO as an effective n-type doped film in a N–P heterojunction silicon-based protocell revealed its feasibility to make up the heterojunction showing its double role as antireflection coating and as substitute of conventional emitters in silicon solar technology. This would open new opportunities of technologically interesting materials fabricated at low manufacturing cost.

1. Introduction

Solar photovoltaic (PV) sector is gaining in competitiveness because of new approaches emerging focused on thickness reduction, kerf avoidance and manufacturing-cost lowering [1]. Data from International Roadmap of Photovoltaic reveal how this sector is experiencing a notable expansion, reached to multiply the installed capacity by a factor of 100 in only 14 years [2]. Despite this, in PV sector, several challenges have yet to be overcome to fully tap the manifold new business opportunities that are now opening up, and therefore new technological progresses are continuously required [3]. The production process is demanding cost-reduction products and reduction of both energy and material losses. Low-temperature fabrication processes compatible with thinner and/or lower-quality wafers are preferred to be incorporated into the production chain [4].

Taking into account that the PV market is currently dominated by wafer-based silicon solar cells production with 90% market share worldwide, a new generation of hybrid devices based on a combination of silicon technology and any of the low temperature developed materials is emerging as key issue of exhaustive investigation. This innovative concept based on the known crystalline Silicon (c-Si) technology presents two main advantages: first, to decrease the number of processing steps; second, to use low temperature in the manufacture. Those innovative concepts were based on by applying semiconductor thin films to replace conventional emitters and/or to act as transparent electrode. The implementation of these complementary selective contacts on silicon absorber would lead to more efficient solar devices [5,6].

Silicon-heterojunction (SHJ)-based solar technology reduces material consumption and processing temperature [7]. In such devices, optical losses are very representative; for this reason, antireflection coatings (ARCs) placed into the front of device play a relevant role [8]. These films must (1) carry out an efficient charge carriers transport to be collected by metallic contacts, and (2) act as effective window layer allowing that most of incident light can reach the Si wafer absorber. Taking these previous requirements into account, transparent conductive oxides (TCOs) are considered as potential choice to be used as ARC. Their morphological and optoelectronic properties are of paramount importance to device performance [9,10]. TCOs are fabricated by many

* Corresponding author.
E-mail address: susanamaria.fernandez@ciemat.es (S. Fernández).

https://doi.org/10.1016/j.vacuum.2020.109783
Received 2 July 2020; Received in revised form 11 September 2020; Accepted 12 September 2020
Available online 16 September 2020
0042-207X/© 2020 Elsevier Ltd. All rights reserved.

different techniques such as pulsed laser deposition, sol-gel, and spray pyrolysis, spin/dip coating or Radio Frequency (RF)/Direct Current (DC) magnetron sputtering processes [11–13]. This last one emerges as one of the most viable technique to deposit large area TCO thin films, and it permits deposition at low temperatures down to room temperature (RT), high deposition rates and good film adhesion to any substrates. In addition, the high energy of the sputtered particles also leads to enhance its mobility at the surface during the deposition, improving the film crystallinity, and consequently, modifying its microstructure [14,15]. Therefore, magnetron sputtering deposition technique presents the reliability and the suitable control for TCO thin films fabrication.

Up to date, indium tin oxide (ITO) fabricated at high temperature is the most commonly used because of its low electrical resistivity and its wide transmission window [16]. In order to achieve crystalline ITO films with good performance, high substrate temperature and/or high temperature post-deposition annealing treatment (400-650 °C) are required [17,18]. However, these crucial steps can lead to raise the energy consumption in the manufacturing process and to damage seriously the subsequent device structure. As far as thin film production by magnetron sputtering is concerned, the most critical parameters are the RF/DC power and the substrate temperature. Both deposition parameters mainly determine the TCO properties that can influence on the performance of the optoelectronic device. Controlling the plasma irradiation damage by using soft power values and low substrate temperatures, the possible device detriment due to that effect can be avoided [19]. At soft sputtering conditions, ITO thin films can present amorphous nature with enhanced transport properties [20]. The decrease of the substrate temperature while materials maintain excellent optoelectronic properties constitute a technological and interesting challenge for the production chain [21,22].

In this work, sputtered ITO thin films were deposited at soft conditions without any post-heat treatment. The influence of the main sputtering deposition conditions, such as substrate temperature and applied power, on material performance was tested to evaluate its potential of developing p-n heterojunction protocells based on silicon technology. Therefore, the main goal of this work is to show the good practice of using ITO thin films, fabricated at low energy consumption sputtering conditions without post-treatment, to replace conventional thin films in silicon heterojunction solar cells technology. The results derived from this investigation have a considerable relevance for enabling to (i) diminish the amount of material, (ii) reduce the energy consumption, and hence, (iii) decrease the production cost.

2. Experimental methods

80 nm nominal-thick ITO thin films were fabricated in a commercial UNIVEX 450B system from Leybold. This system is equipped with magnetron sources, two of them operated by Radio Frequency (RF) and the rest ones, operated by direct current (DC). The four guns are placed in a confocal geometric configuration at around 0.15 m from substrate to assess the film homogeneity. The material deposition was performed on both 4-inches polished resistive float zone <100> silicon wafer (resistivity>10^4 Ω-cm) and 10 × 10 cm^2-size Corning glass. The silicon substrate was used to determine the nature, the chemical composition, the antireflection capability (AR) and the electrical parameters of the ITO thin films. On the other hand, the glass substrate was used to corroborate their nature and determine the main optical parameters.

Prior to load the substrate into the load-lock, it was cleaned by different ways: the silicon wafer was chemically etched using a dilute (2%) hydrofluoric acid to remove the native oxide SiO_x from its surface, rinsed in deionized water (D.I.W.) and dried by blowing nitrogen over it; and the glass was ultrasonically cleaned with DECON 90 detergent, rinsed in DIW, immersed for 2 min in isopropyl alcohol and finally, dried.

Prior to the sputtering deposition, an Argon plasma bias etching on the substrates was carried out without intentional heating at 120 W at 0.5 Pa for 5 min. The goal of this step was to improve the material adherence to the substrate. The sputtering process was carried out at oxygen free with a base pressure close to 1×10^{-5} Pa. The Argon gas used had a purity of 99.999% and its flux was controlled by MKS mass flow controller. During the deposition, the substrate was rotated at 20 rpm, and the gas flow rate and working pressure were set at 5 sccm and 0.17 Pa, respectively. The values of the DC power (DCP) applied to the ITO target was ranged from 15 to 100 W; while the substrate temperature was set to room temperature (RT). The nominal thickness of the sputtered thin films was 80 nm-thick because of the envisaged applications as ARC in the silicon-based devices technology. To evaluate the effect of both the substrate temperature and the DCP on the thin film properties, a nominal 80 nm-thick ITO thin film was deposited at 190 °C and 75 W, respectively, labelled as reference sample.

Structural composition was determined by powder X-Ray diffraction (XRD). The patterns were obtained by using a PANalytical X'Pert Pro diffraction system configured with a vertical Thetha wide angle goniometer. This goniometer operates in grazing incidence (GI) configuration using a Goebel-type parallel beam mirror on the incident beam side, and a linear X'Celerator detector in receiving slit mode attached to a parallel plate collimator on the diffracted beam side. The CuK_α radiation (45 kV - 40 mA) was used at a fixed incident angle of $\omega = 2.5^\circ$ in parallel beam geometry, in an angular range of $20^\circ < 2\theta < 80^\circ$. Phase identification was obtained by comparison with The Inorganic Crystal Structure Database (ICSD). Crystallite size (D) was also obtained from Scherrer formula [23].

$$D = 0.94\lambda/\beta\cos\theta \tag{1}$$

where λ is the wavelength of the X-ray used, θ is the Bragg diffraction angle, and β is the full-width-at-half-maximum (FWHM) in radians.

For wavelength dispersive X-ray fluorescence analysis (WDXRF), a PANalytical AXIOS automated XRF spectrometer was used to determine the elemental composition. The samples did not require any preparation, and the data were interpreted by making use of a semiquantitative (OMNIAN) method, developed by PANalytical.

The film morphology was analysed using a Digital Instruments Nanoscope IIIa Atomic Force Microscope in tapping mode with Bruker NCHV probes. The 2 × 2μm^2 scans were processed using Nanotec software WSxM [24]. Hall mobility and carrier concentration were obtained by the Van der Pauw method under a 1.2 T magnetic field at RT.

The optical transmittance (T) spectra were measured at RT and normal incidence in the wavelength range from 300 to 2500 using a UV/Visible/NIR PerkinElmer Lambda 1050 spectrophotometer. The films absorption coefficient (α) was calculated from the optical transmission (T) by the following equation (2)

$$\alpha = (\ln 1/T)/\ d \tag{2}$$

where d is the film thickness, and (hv) the photon energy. The absorption coefficient (α) and incident photon energy (hν) are related by the following relation [25]:

$$(h\nu\alpha)^2 = A(h\nu - E_g) \tag{3}$$

where A is a constant and E_g is the optical band gap. Therefore, the E_g values were determined by extrapolation of the straight section of the $(\alpha h\nu)^2$ versus hν. In addition, the AR capability of the thin films was determined from the hemispherical reflectance spectra R_{hem} measured with the UV/VIS/NIR PerkinElmer Lambda 1050 spectrophotometer equipped with the 6 mm integrated sphere accessory.

Finally, the ITO thin film performance was evaluated from the figure of merit (FOM), φ_{TC}, proposed by Haacke [26] given by

$$\varphi_{TC} = T^{10}/R_s \tag{4}$$

where, T is the average optical transmittance and R_s is the sheet resistance.

The ITO thin films were used to fabricate ITO/p-Si heterojunctions

protocells. These devices were fabricated onto polished FZ p-type silicon substrates (resistivity~ 1000-5000 Ω-cm). A metallic grid of Ti (55 nm)/Ag (1 μm) was used as front contact, and 900 nm-thick aluminum layer was used as rear contact. This last one was previously annealed at 350 °C for 2 h in Argon environment to achieve an ohmic behaviour. The current-voltage (JV) characteristics of the devices were measured under illumination calibrated at AM1.5G conditions and 100 mW/cm^2, using a class A solar simulator (Steuernagel SC575).

3. Results

3.1. ITO thin films fabricated at RT

Fig. 1 shows the deposition rate tendency with the DCP in the range of values used. A linear increase of the deposition rate with the DCP was observed, as expected.

Fig. 2 pictures the GI-XRD patterns of the as-deposited 80 nm-thick ITO films. As it can be noticed, a transition from amorphous to crystalline nature happened with the increase of the DCP [27,28]. The thin films deposited at 15 and 25 W showed a broad shoulder around 31° that confirmed the amorphous nature. Otherwise, samples deposited at DCP values higher than 25 W showed polycrystalline (pc) structure, with the appearance of different diffraction peaks. This change in the crystal phase observed was attributed to the gradual enhancement of the adatom mobility obtained as power increased, considering the low-temperature regimen used in the deposition in this work.

In addition, no characteristic peaks of Sn, SnO or SnO_2 were observed in the scans, meaning the right substitution of the indium (In) cation by the tin (Sn) cation in the cubic lattice [29]. The diffraction peaks corresponding to (222), (440) and (622) planes appeared more intense [29,30], being the (222) plane, corresponding to the cubic bixbyite In_2O_3, that presented the strongest intensity that increased with the DCP. This (222) preferential plane was related to a change in kinetic energy of the particles that reach the growth front due to the growth conditions employed: RT and low regime of power irradiation. Less intense diffraction peaks such as (211), (400), (411), (332), (431) and (611) were also observed [30,31], supporting the pc nature, and revealing the random orientation of the films. Fig. 2 also includes the pattern of the reference sample that also showed a pc nature. For this sample, the (611) plane was the most intense, while the (222) and (400) peaks were almost negligible.

The grain size of the pc thin films was calculated from the width of the main (222) reflection peak using formula (1). The obtained values were close to 10–12 nm, regardless the deposition conditions. These small values were attributed to the low substrate temperature and to the

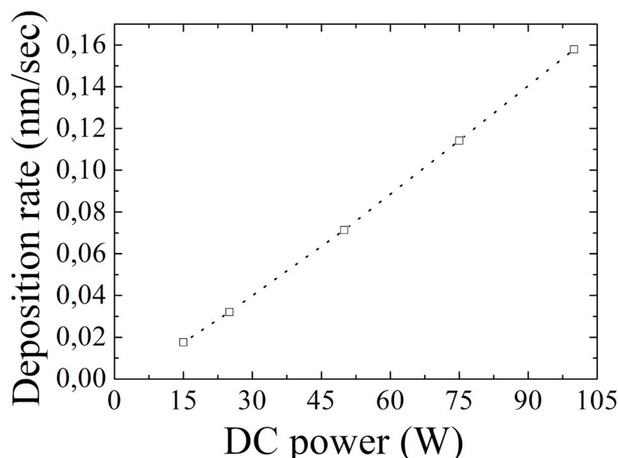

Fig. 1. Deposition rate as function of DC power value used in ITO film deposition.

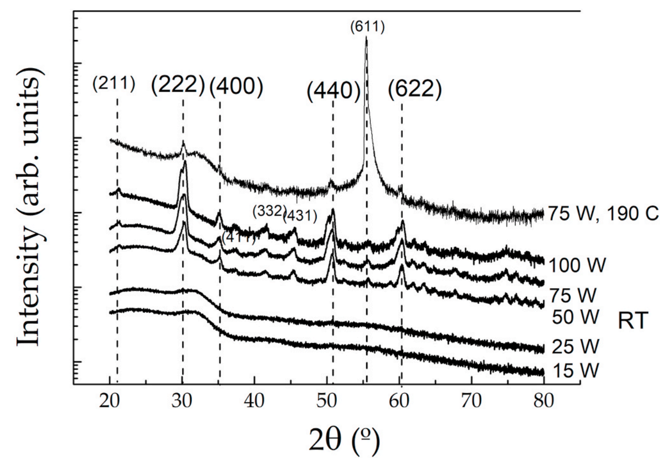

Fig. 2. GI-XRD scans of 80 nm-thick ITO thin films deposited on Corning glass at RT and different DC powers. The reference ITO sample deposited at 190 °C and 75 W was also included.

quite small thickness of the films (~80 nm). These values were comparable to the state-of-art of thin ITO films deposited at such conditions of temperature and thickness [32].

Table 1 shows the chemical composition (in percentage) for each element of the ITO thin films as function of DCP, also including the chemical analysis carried out to the ITO ceramic target used in this work. These chemical data were estimated from WD-XRF measurements. Moreover, the data related to the considered as reference ITO thin film (deposited at 190 °C and 75 W), and the intensity ratio between (222) and (400) planes extracted from XRD spectra were also included in Table 1. First, it can be noticed that the samples can be divided in two groups, depending on the film crystalline nature: the amorphous and the pc phases, respectively. Within each group, the elemental composition of In, Sn and O, respectively, slightly changed as function of DCP. . In both films groups, the most appreciable increase with the DCP was showed by the Sn composition, while the In and O compositions presented the reverse tendency. Moreover, the In/Sn ratio decreased with the DCP while the O/In ratio was maintained almost constant. This could point to an effective introduction of Sn into lattice with the ITO target power, favoured by the increase of the deposition rate with that sputtering parameter (as pointed out Fig. 1). A similar behaviour has been already observed in other materials [33]. As it can be observed, the chemical composition of each element was not so far than the showed by the raw material (ceramic target). These slight differences from the raw material can be attributed to the changes in the deposition conditions such as the DCP.

On the other hand, the highest (222)/(400) peak intensity ratio obtained from XRD patterns of the pc thin films was reached in that sample with the highest Sn composition (hence, lowest In/Sn chemical composition ratio). The introduction of the Sn into lattice seems to lead to an improvement of the film crystallinity. In addition, the rising

Table 1
Evolution of the chemical composition in percentage for each element determined by WD-XRF in the nominal 80 nm-thick ITO thin films in study.

DCP (W)	In (%)	Sn (%)	O (%)	$I_{(222)}$/ $I_{(400)}$	In/Sn	O/ In
15	76.0 ± 0.5	6.2 ± 0.5	17.8 ± 0.5	–	12.26	0.23
25	74.2 ± 0.7	8.8 ± 0.8	17.0 ± 0.5	–	8.43	0.23
50	76.0 ± 0.3	5.9 ± 0.5	18.1 ± 0.4	2.91	12.88	0.24
75	74.9 ± 0.6	7.5 ± 0.7	17.6 ± 0.5	3.80	9.98	0.23
100	74.5 ± 0.4	8.2 ± 0.4	17.3 ± 0.3	4.97	9.08	0.23
Ref. 75*	76.0 ± 0.4	5.5 ± 0.5	18.5 ± 0.6	1.98	13.81	0.24
Target	76.0	6.0	18.0	–	12.67	0.24

tendency of the (222)/(400) peak intensity ratio with the DCP was related to the enhancement of the kinetic energy of the sputtered particles when DCP increased. This fact affects the surface migration of arriving particles, leading to favour the incorporation of Sn into the lattice, in agreement with WD-XRF results. Moreover, That enhancement of the kinetic energy with DCP, converted into thermal one at the substrate surface, is the responsible for the improvement of film crystallinity, as supported the increase of the (222)/(400) intensity ratio obtained from the XRD patterns of the pc thin films [28].

Atomic force microscope (AFM) in tapping mode was used to evaluate the topography of the thin film surfaces. Fig. 3 depicts the 2-dimensional (2D) AFM micrographs of 80 nm-thick ITO films deposited at RT and different DCP values. Table 2 summarizes the roughness (measured in root-mean-square (RMS)), the density and the height of the protrusions observed on the surfaces, determined with the WSxM software [24,34]. Two different morphologies were observed depending on the film nature, regardless the slight chemical composition changes observed by WD-XRF measurements. The surfaces of the amorphous thin films were very smooth with a slight presence of protrusions on it, and RMS values in the order of Å, attributed to its amorphous nature [35]. For pc thin films, the surfaces were rougher with RMS values close to 1.1 nm. Many protrusions of different dimensions were observed on these surfaces. That increase in the roughness was attributed to the increase of kinetic energy of the sputtered particles at the pc regimen [34]. Table 2 also includes the percentage of covered surface by the protrusions, determined from the AFM micrographs. The results indicated that the area covered by the protrusions and their density were more than 50 times higher, while the protrusions height was almost 3 times higher on the pc thin films, in agreement with the higher RMS reached in these samples. The reference ITO layer also showed protrusions of 2 nm-height covering a lower surface area of 5.5% compared with the pc thin films deposited at RT. This decrease was attributed to the influence of substrate temperature on the motion of the sputtered particles, enhancing their kinetic energy. This effect would affect the film morphology, leading to slightly smoother surfaces with lower density of protrusions [36] compared with the films deposited at RT. Therefore, so far, the amorphous ITO thin films with free-protrusions smooth surfaces can be considered suitable to be used as electrode into device.

Table 2
Morphological parameters derived from the AFM measurements in the nominal 80 nm-thick ITO thin films as function of the DCP. (*) ITO reference thin film deposited at 190 °C.

DCP (W)	Covered surface (%)	Density (μm^{-2})	Height/RMS (nm)	Nature
15	0.2	2.75	1.0/0.10	Amorphous
25	0.5	3.25	2.5/0.24	Amorphous
50	22.6	170	8.0/1.10	pc
75	8.7	120	2.0/0.50	pc
75*	5.5	30	2.0/0.35	pc

Table 3 summarizes the electrical data as function of the thin film nature obtained from Hall measurements. A subtle dependence on the carrier concentration with the film nature was appreciated. The pc-ITO thin films showed both slightly higher carrier mobility μ and carrier concentration n in comparison with amorphous film ones. Both facts

Table 3
Electrical parameters of nominal 80 nm-thick ITO thin films deposited at RT on resistive c-Si wafers. (*) ITO reference thin film deposited at 190 °C.

DCP (W)	n (10^{20} cm^{-3})	μ (cm^2/Vs)	ρ x 10^{-3} (Ω-cm)	Nature	O (%)/Sn (%)
15	6.2	17.3	1.1	Amorphous	17.8 ± 0.5/6.2 ± 0.5
25	7.2	16.0	1.0	Amorphous	17.0 ± 0.5/8.8 ± 0.8
50	12.4	18.7	0.85	pc	18.1 ± 0.4/5.9 ± 0.5
75	7.2	16.5	0.80	pc	17.6 ± 0.5/7.5 ± 0.7
100	10.2	19.0	0.65	pc	17.3 ± 0.3/8.2 ± 0.4
75*	6.1	18.6	0.70	pc	18.5 ± 0.6/5.5 ± 0.5

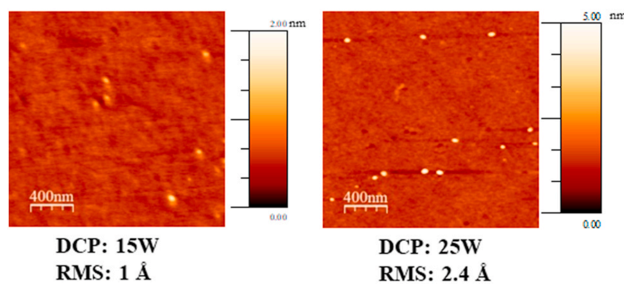

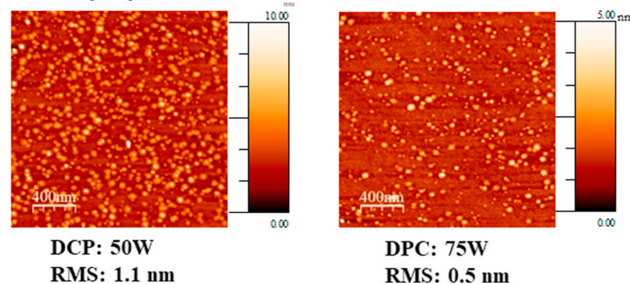

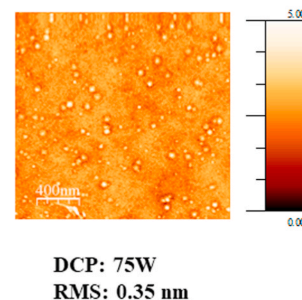

Fig. 3. 2D surface topography images of 80 nm-thick ITO film samples deposited at RT and different DC powers: a) amorphous materials, b) polycrystalline materials and c) reference sample (190 °C, 75 W).

were attributed to the effect of DCP on: (i) the film crystallinity improvement, supported by the increase of the intensity ratio between (222) and (400) planes as DCP increased [12] extracted from data in Table I, and (ii) the increase of oxygen deficient into the film [37]. In amorphous thin films, it is well stablished that the Sn doping did not contribute to generate carriers [38] since the Sn atoms would be mostly placed at interstitial positions. As DCP increases and the amorphous nature turned into pc, the Sn atoms could be diffused from interstitial to In cation sites, replacing them. At the same time, in that structural transition, the realignment of In–O bonds would be going on to generate a locally ordered structure. This realignment would be shorter than a single bixbyite unit cell, but sufficiently organised in InO_6 structural units to allow the creation of oxygen vacancies that would contribute to carrier increase [11]. Both effects, the cation substitution and the creation of oxygen vacancies, could be the reason of the relevant drop in carrier concentration from 7.2×10^{20} cm^{-3}, showed by the amorphous thin film deposited at 25 W, up to 12.4×10^{20} cm^{-3}, measured in the pc thin film deposited at 50 W. In addition, the low resistivity observed in this sample was attributed to that increase of the carrier concentration. On the other hand, the slight variation in the mobility observed in the pc thin films might be due to the grain boundary scattering, ionized impurity scattering and the network modifications resulting from doping content. This fact can be related to the decrease of oxygen and the increase of Sn concentrations, respectively, with the DCP derived from WD-XRF measurements and listed in Table 3 [39]. The reference ITO thin film deposited at the high energy conditions of 190 °C and 75 W presented a mobility of 18.6 cm^2/V, close to the pc material fabricated at RT, but with a relative lower carrier concentration. In this case, the resistivity of this sample was the lowest, attributed to that high mobility.

With regards to the optical performance, Fig. 4 a) shows the normalised transmission spectra of the nominal 80 nm-thick ITO thin films as function of ITO DCP. The spectrum of reference sample was also included (represented by filled square symbols). It is noticed that average transmittance in the visible region of the amorphous samples

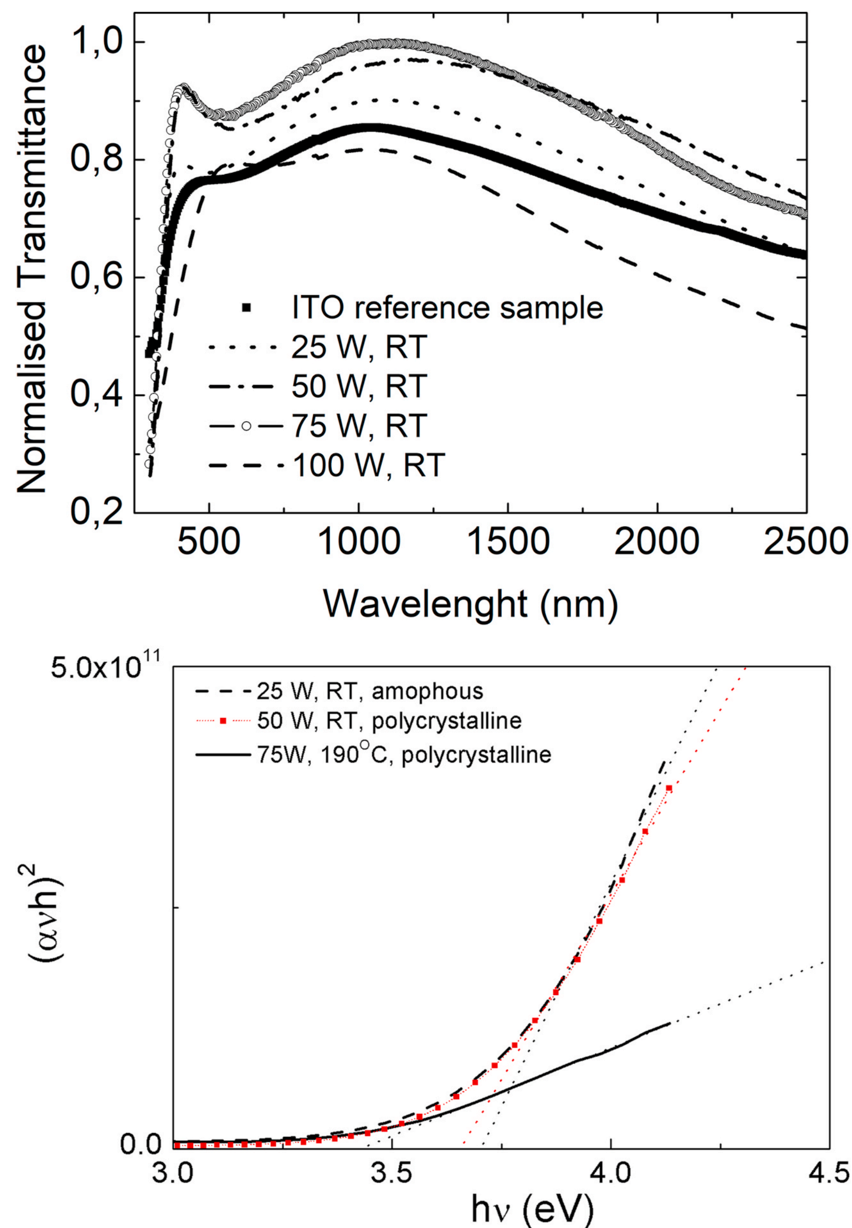

Fig. 4. a) Normalised transmission spectra of the nominal 80 nm-thick ITO thin films as function of the ITO DCP, and b) $(\alpha h\nu)^2$ versus photon energy ($h\nu$) to calculate the band gap energy values of the thin films prepared at the sputtering conditions that lead to the transition from amorphous to pc nature, 25 W and 50 W, respectively. The reference sample (190 °C, 75 W) is included in both for comparison.

was relatively lower than for pc films. Despite this, that value was higher than 0.8 in all cases, except for the sample deposited at 100 W and RT. As the DCP increased from 25 W to 50 W, the films suffered a transition from amorphous to crystalline phase that resulted in increased grain size, in agreement with XRD results. Therefore, the observed slight enhancement of the transmittance at that stage, from 0.81 to 0.85, can be attributed to the crystallinity improvement [40] and to the slightly higher Sn concentration showed by the pc film deposited at 50 W (see data in Table 3). In the pc regimen and as AFM analysis pointed out, the higher sputtering DCP the smoother surface was obtained, what would lead to the increase of the average transmittance reached by the sample deposited at RT and 75 W. This is attributed to the reduction of light scattering on this smoother surface and to its better crystalline structure as revealed its highest (222)/(400) intensity ratio showed in Table 1 [41]. With regards to the sample deposited at 100 W, an important detriment in the average transmittance was observed. This may be due to two effects: First, the measured thickness of 100 nm, slightly higher than the nominal one. Second, the slightly higher Sn content compared with the rest of pc samples.

Fig. 4 b) plots $(\alpha h\nu)^2$ versus photon energy ($h\nu$) to calculate the optical band gap energy E_g of the thin films deposited at the different ITO DCP of 25 W and 50 W, the parameters that led to the amorphous to pc transition. For comparison, the plot of $(\alpha h\nu)^2$ for the reference sample was also included. The extrapolation of the straight-line portion of the plot of $(\alpha h\nu)^2$ to zero absorption gives the direct band gap of the thin films. The values of E_g calculated for the samples in study are summarized in Table 4. The widening of E_g observed with the DCP in the amorphous thin films may be related to the increase of the carrier concentration; and, hence, may be explained by using Moss–Burstein effect [42]. In the transition point, the observed red shift in E_g may be due to the increasing of the carrier concentration, as supported the electrical data from Table 3, and in agreement with the results showed by other authors [40]. On the other hand, in the pc regime, the obtained E_g decreased when increased the DCP. This narrowing would be related to the increase of the Sn concentration that would lead to many-body interaction effects either between free-carriers or between free-carriers and ionized impurities [40]. Finally, the reference sample deposited at 190 °C and 75 W showed a very poor transmittance of 0.71 and a narrow band gap energy of 3.42 eV. These behaviours could be explained because of the change in the texture to (611) preferred direction provided by at the regime of the high energy consumption deposition conditions used in this sample, as it was suggested by Higuchi et al. [43,44]. As a summary, the better optoelectronic properties were reached for films deposited at low energy consumption conditions in a free-oxygen environment. For photovoltaic applications, ITO thin films must have both low resistivity and high optical transmittance. In order to determine the more suitable deposition conditions to achieve the best performance, the FOM were calculated. These values as function of the DCP are listed in Table 4. As it can be noticed the highest value of 34.9 × 10^{-4} Ω^{-1} was reached by the pc sample deposited at 75 W, followed by 18.2 × 10^{-4} Ω^{-1} corresponding to the sample deposited at 50 W. On the other hand, the reference sample showed the lowest FOM value. Finally,

Table 4
Average optical transmittance, optical band gap energy and the figure of merit (FOM) calculated for nominal 80 nm-thick ITO thin films deposited at RT on the resistive Corning. The data of ITO reference sample (*) are also included for comparison.

DCP (W)	Normalised $T_{400–800\ nm}$	E_g (eV)	FOM (x 10^{-4} Ω^{-1})	Nature
15	0.83	3.61	11.3	Amorphous
25	0.81	3.70	9.7	Amorphous
50	0.85	3.65	18.2	pc
75	0.90	3.63	34.9	pc
100	0.77	3.15	9.0	pc
75*	0.71	3.42	3.7	pc

the best morphology was achieved by the amorphous samples deposited at low DCP of 15 and 25 W, but the best FOM value was reached by the pc sample deposited at 75 W and RT. It can be concluded that the more relevant limiting factor was the substrate temperature. In order to evaluate the performance of these films on a device, n-p heterojunctions based on them were fabricated on silicon.

3.2. N–P heterojunctions based on ITO fabricated at low temperature

80 mn-nominal thick ITO thin films were used to develop n/p-Si heterojunction solar protocells using polished FZ p-type silicon as absorber layer. The ITO thin films used in these devices were previously described in the 3.1 section. Fig. 5 plots the J-V characteristics measured under illumination of the protocells fabricated. In general, a rectifying behaviour was obtained, regardless of the ITO thin films properties. I. It should be noticed that no passivation layer was used with the goal of evaluating and discriminating the effect of the quality of ITO thin films on the device performance.

Table 5 lists the main electrical device parameters, J_{sc}, V_{oc}, the ITO thickness of the films measured with a profilometer and the average hemispherical reflectance calculated in the visible wavelength range. The sputtering deposition conditions such as the DCP and the substrate temperature, and the nature of the thin films were included as guide to analyse the data. The results indicated that the highest V_{oc} of 0.224 V was achieved by the protocell fabricated with the pc ITO thin film deposited at RT and at 75 W, followed very closely by the device with the pc film deposited at RT and at 50 W, reaching a V_{oc} of 0.218 V. These results are in very good agreement with the best FOM values obtained for these samples in section 3.1. In the case of using amorphous ITO thin films in the protocells, the highest V_{oc} of 0.214 V was obtained when the film was deposited at RT and 15 W. That value was also very close to the results obtained by the devices with pc thin films. Besides it followed the tendency for those samples obtained in the performance analysis carried out by the FOM values. The device fabricated with the ITO reference sample (190 °C and 75 W) showed a very low value of V_{oc}, demonstrating the strong detrimental effect of the substrate temperature on the device performance. Despite this, the lack of a passivating layer on silicon was the main responsible of the low V_{oc} values.

On the other hand, the J_{sc} was affected by the optical losses. These losses would consider the number of photons reflected on the protocell surface and those absorbed by ITO layer (i.e. free carrier absorption), because they did not reach the silicon absorber [45]. Therefore, the ITO

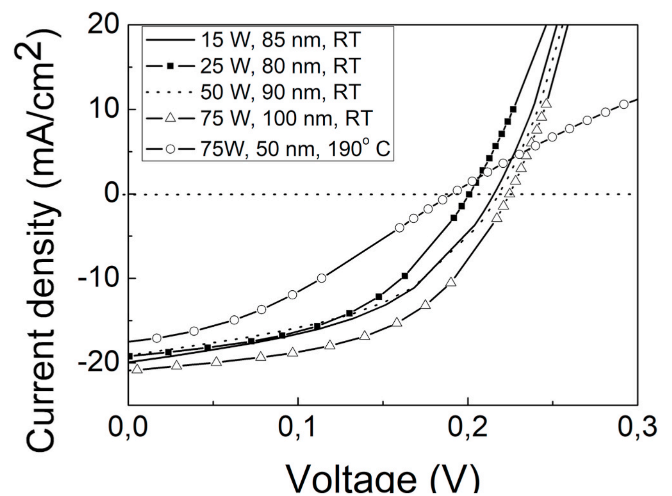

Fig. 5. J-V characteristics measured under illumination of the protocells fabricated with ITO thin films fabricated at RT and different DCP values. The protocell fabricated with the reference sample deposited at 190 °C and 75 W was included for comparison.

Table 5
Open circuit voltage V_{oc} and short circuit current J_{sc} extracted from J-V characteristics obtained under illumination of the protocells fabricated with different ITO thin films. Average hemispherical reflectance values at 400–800 nm wavelength range are included to analyse the amount of light that pass through the device to silicon absorber. (*) ITO reference thin film deposited at 190 °C.

DCP (W)	d (nm)	$T_{substrate}$ (°C)	V_{oc} (mV)	J_{sc} (mA/cm^2)	R_{hem} (%)	FF (%)
15	85.0	RT	0.214	19.8	13.3	49.7
25	80.0	RT	0.20	19.2	11.9	48.1
50	90.0	RT	0.218	19.2	15.6	50.2
75	100.0	RT	0.224	20.8	18.5	50.8
75*	50.0	190 °C	0.18	17.6	20.5	45.6

thin films were playing two roles in the protocells fabricated in this work: The first one, to constitute the p-n heterojunction, confirmed by the J-V measurements, and the second one, to act as AR coating, demonstrated by the average total (hemispherical) reflectance. Fig. 6 pictures the total (hemispherical) reflectance spectra of the fabricated protocells. In the inset of this figure, the variation of the average hemispherical reflectance values, calculated in the wavelength range of 400–800 nm, with the measured ITO thickness is plotted. As it can be appreciated, a minimum R_{hem} value was achieved at the ITO thickness of 80 nm, in agreement with theoretical predictions [46]. In addition, as the thickness moved away from the stablished optimum film thickness to be an effective AR coating [45,47], R_{hem} increased. In all cases, the incorporation of ITO thin film led to that the average R_{hem} value managed to decrease below the light reflection on silicon surface of 30%. The slight changes observed in J_{sc} were attributed to the different absorption coefficients of the ITO thin films obtained with the sputtering deposition conditions.

These data demonstrate the feasibility of low energy fabrication of ITO for low-cost silicon-based solar technology.

4. Conclusions

80 nm-nominal thick ITO thin films were prepared by DC magnetron sputtering at RT and in a range of DCP from 15 to 100 W. The XRD patterns showed a transition from amorphous to polycrystalline nature with cubic structure at a DCP of 50 W. The crystallite size of the pc films varied from 10 to 12 nm. The AFM images of thin films showed very smooth and free-protrusions surfaces for the amorphous thin films, and rougher surfaces with the appearance of protrusions on the surface of the pc films. In fact, at the transition point, the density of these protrusions was the highest and it was decreased as the DCP increased. The calculated band gap energies E_g decreased from 3.7 eV to 3.65 eV in the nature transition point due to the increase of the carrier concentration; in the pc regime, a red-shift of E_g was also observed attributed to the increase of Sn concentration as a result of the occurrence of additional energetic levels in the forbidden gap. The average transmittance of the most of thin films was higher than 0.8, and the FOM calculated showed the best performances for the thin films deposited at RT and at DCP as follows: 75 W, 50 W and 15 W. Finally, the potential of ITO layer deposited at low energy consumption regime was demonstrated fabricating protocells based on a n-p heterojunction ITO/p-Si. The influence on solar device parameters as function of deposition parameters of ITO film used in its fabrication was presented. The results showed the effectiveness of ITO material as AR coating and as a possible substitute of the conventional emitters used in silicon-based technology.

Credit author statement

Susana Fernández: Conceptualization, Methodology, Investigation, Writing- Original draft preparation, Supervision. José Pablo González, Fernando García, Fernando Borlaf, Javier Grandal, Alejandro F. Braña,

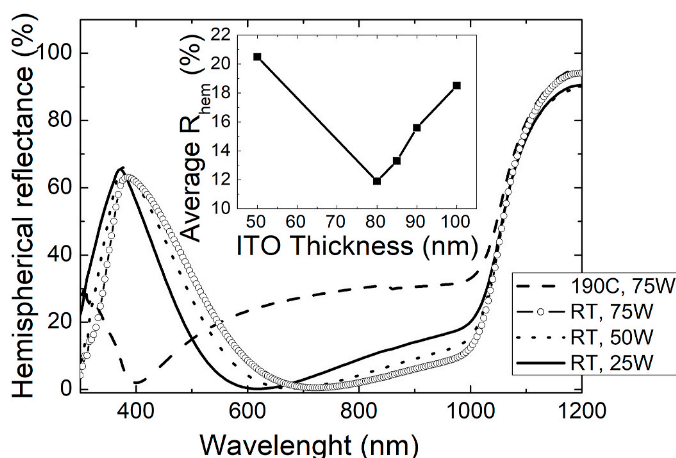

Fig. 6. Hemispherical reflectance spectra of the protocells fabricated with ITO thin films fabricated at RT and different DCP values. In the inset, the variation of the average hemispherical reflectance calculated in the wavelength range of 400–800 nm, with the ITO thickness used into the devices.

M. Belén Gómez-Mancebo: Investigation, Data curation, Validation. Javier Grandal, Alejandro F. Braña, M. Belén Gómez-Mancebo: Writing-Reviewing and Editing.

Declaration of competing interest

The authors declare that they have no known competing financial interests or personal relationships that could have appeared to influence the work reported in this paper.

Acknowledgment

Partial financial support was provided by the Spanish Ministry of Economy and Competitiveness under CHENOC project (ENE2016-78933-C4-3-R).

References

[1] W. Sark, L. Korte, F. Roca, Physics and Technology of Amorphous-Crystalline Heterostructure Silicon Solar Cells, Springer, Berlín, Heidelberg, 2012, ISBN 978-3-642-22275-7, pp. 1–12, https://doi.org/10.1007/978-3-642-22275-7_1, 978-3-642-22274-0.
[2] https://itrpv.vdma.org.
[3] Global Market Outlook for Solar Power 2018 - 2022. https://www.solarpowereurope.org/.
[4] https://www.pv-magazine.com/2019/10/26/the-weekend-read-a-lead-free-future-for-solar-pv/.
[5] F. Feldman, M. Simon, M. Bivour, C. Reichel, M. Hermle, S.W. Glunz, Carrier selective contacts for Silicon solar cells, Appl. Phys. Lett. 104 (May 2014) 181105 (1)–181105(4), https://doi.org/10.1063/1.4875904.
[6] D.L. Young, W. Nemeth, S. Grover, A. Norman, H.-C. Yuan, B.G. Lee, V. LaSavia, P-Stradins, Carrier selective, passivated contacts for high efficiency silicon solar cells based on transparent conductive oxides, IEEE 40th Photovoltaic Specialist Conference (PVSC) 55 (October 2014) 733–740, https://doi.org/10.1109/PVSC.2014.6925147.
[7] C. Battaglia, A. Cuevas, S. De Wolf, High efficiency crystalline silicon solar cells: status and perspectives, Energy Environ. Sci. 9 (February 2016) 1552–1576, https://doi.org/10.1039/c5ee03380b.
[8] H.K. Raut, A.G. Venkatesan, S. Nair, S. Ramakrishna, Anti-reflective coatings: a critical, in-depth review, Energy Environ. Sci. 4 (10) (August 2011) 3779–3804, https://doi.org/10.1039/C1EE01297E.
[9] P. Jayaram, Multication Transparent Conducting Oxides: Tunable Materials for Photovoltaic Applications: Silicon & beyond, Scrivener Publishing LLC, Wiley Online Library, 2019, https://doi.org/10.1002/9781119407690.ch8. Online ISBN: 9781119407690.
[10] A. Stadler, Transparent conducting oxides—an up-to-date overview, Materials 5 (4) (April 2012) 661–683, https://doi.org/10.3390/ma5040661.
[11] S. Fernández, F.B. Naranjo, Optimization of aluminum-doped zinc oxide films deposited at low temperature by radio-frequency on flexible substrates for solar cell applications, Sol. Energy Mater. Sol. Cells 94 (August 2009) 157–163, https://doi.org/10.1016/j.solmat.2009.08.012.

[12] M. Thirumoothi, J.T.J. Prakash, Structure, optical and electrical properties of indium tin oxide ultra thin films prepared by jet nebulizer spray pyrolysis technique, J. Asian Ceram. Soc. 4 (January 2016) 124–132, https://doi.org/10.1016/j.jascer.2016.01.001.
[13] Z. Chen, W. Li, R. Li, Y. Zhang, G.Q. Xu, H. Cheng, Fabrication of highly transparent and conductive ITO thin films with a high figure of merit via solution processing, Langmuir 29 (45) (October 2013) 13836–13842, https://doi.org/10.1021/la4033282.
[14] Y.S. Jung, D.W. Lee, D.Y. Jeon, Influence of dc sputtering parameters on surface morphology of indium tin oxide thin films, Appl. Surf. Sci. 221 (June 2003) 136–142, https://doi.org/10.1016/s0169-4332(03)00862-6.
[15] Z.A. Wang, H.B. Zhu, D.W. Zhang, J.H. Shi, X.D. Li, W.J. Cheng, Z. Sun, S. M. Huang, Stability of transparent conducting oxide films deposited by sputtering for solar cells applications. 34th IEEE Photovoltaic Specialists Conference, PVSC), Philadelphia, PA, February 2010, https://doi.org/10.1109/PVSC.2009.5411587, 000676-000679.
[16] A. Lebbad, L. Kerkache, A. Layadi, F. Leroy, B. Alshehri, E. Dogheche, Surface morphology, structural and electrical properties of RF-Sputtered ITO thin films on Si substrates, Bull. Mater. Sci. 41 (9) (May 2018) 74, https://doi.org/10.1007/s12034-018-1595-1.
[17] P. Prepelita, I. Stavarache, D. Craciun, F. Garoi, C. Negrila, B.G. Sbarcea, V. Craciun, Rapid thermal annealing for high-quality ITO thin films deposited by radio-frequency magnetron sputtering, Beilstein J. Nanotechnol. 10 (July 2019) 1511–1522, https://doi.org/10.3762/bjnano.10.149.
[18] N.M. Ahmed, F.A. Sabah, H.I. Abdulgafour, A. Alsadig, A. Sulieman, M. Alkhoaryef, "The effect of post annealing temperature on grain size of indium-tin-oxide for optical and electrical properties improvement" Results in Physics, 13, February 2019, p. 102159, https://doi.org/10.1016/j.rinp.2019.102159, 6.
[19] V. Linss, M. Bivour, H. Iwata, K. Ortner, Comparison of low damage sputter deposition techniques to enable the application of very thin a-Si passivation films, AIP Conf. Proc. 2147 (August 2019), 040009, https://doi.org/10.1063/1.5123836.
[20] D.C. Paine, T. Whitson, D. Janiac, R. Beresford, C.W. Ow-Yang, B. Lewis, A study of low temperature crystallization of amorphous thin film indium-tin-oxide, J. Appl. Phys. 85 (12) (March 1999) 8445–8450, https://doi.org/10.1063/1.370695.
[21] S. Fernández, F. Borlaf, F. García-Pérez, M.B. Gómez-Mancebo, C. Munuera, M. García-Hernández, H. Elhouichet, A.F. Braña, F.B. Naranjo, Mater. Sci. Semicond. Process. 90 (October 2018) 252–258, https://doi.org/10.1016/j.mssp.2018.10.027.
[22] J.D. Perkins, T. Gennett, M. Galante, D. Gillaspie, D. Ginley, "Amorphous Indium-Zinc-Oxide Transparent Conductors for Thin Film PV", 37th IEEE Photovoltaic Specialist Conference (PVSC), 2011, pp. 3646–3648, https://doi.org/10.1109/PVSC.2011.6185939.
[23] B.D. Cullity, Elements of X-Ray Diffraction, Addison-Wesley, Reading, 1978.
[24] I. Horcas, R. Fernández, WSXM: a software for scanning probe microscopy and a tool for nanotechnology, Rev. Sci. Instrum. 78 (January 2007), https://doi.org/10.1063/1.2432410, 013705 (8 pages).
[25] M. Thirumoorthi, J. Thomas, J. Prakash, "Structural, morphological characteristics and optical properties of Y doped ZnO thin films by sol–gel spin coating method", Superlattice. Microst. 85 (September 2015) 237–247, https://doi.org/10.1016/j.spmi.2015.05.005.
[26] G. Haacke, New figure of merit for transparent conductors, J. Appl. Phys. 47 (September 1976) 4086, https://doi.org/10.1063/1.323240.
[27] V. Malathy, S. Sivaranjani, V.S. Vidhya, J.J. Prince, T. Balasubramanian, C. Sanjeeviraja, M. Jayachandran, Amorphous to crystalline transition and optoelectronic properties of nanocrystalline indium tin oxide (ITO) films sputtered with high rf power at room temperature, J. Non-Crys. Sol. 355 (June 2009) 1508–1516, https://doi.org/10.1016/j.jnoncrysol.2009.04.043.
[28] K.A. John, R.R. Philip, P. Sajan, T. Manju, In situ crystallization of highly conducting and transparent ITO thin films deposited by RF magnetron sputtering, Vacuum 132 (July 2016) 91–94, https://doi.org/10.1016/j.vacuum.2016.07.035.
[29] N.M. Ahmeda, F.A. Sabaha, H.I. Abdulgafour, A. Alsadig, A. Sulieman, M. Alkhoary, The effect of post annealing temperature on grain size of indium-tin-oxide for optical and electrical properties improvement, Results Phys. 13 (6) (February 2019) 102159, https://doi.org/10.1016/j.rinp.2019.102159.
[30] J. Pannetier, G. Denes, Tin(II) oxide: structure refinement and thermal expansion, Acta Crystallogr. B 36 (November 1980) 2763, https://doi.org/10.1107/S0567740880009934.
[31] V.M. Goldschmidt, T. Barth, G. Lunde, Isomorphie und Polymorphie der Sesquioxyde. Die Lanthaniden-Kontraktion und ihre Konsequenzen, Skr. Nor. Vidensk.-Akad., Mat.-Naturvidensk. Kl. (7) (1925) 1–59.
[32] O. Tuna, Y. Selamet, G. Aygun, L. Ozyuger, High quality ITO thin films grown by DC and RF sputtering without oxygen, J. Phys. D Appl. Phys. 43 (January 2010), https://doi.org/10.1088/0022-3727/43/5/055402, 055402 (7 pages).
[33] D.-C. Tsai, Z.-C. Chang, B.-H. Kuo, C.-M. Chen, E.-C. Chen, F.-S. Shieu, Influence of chemical composition on phase transformation and optoelectronic properties of Cu–Cr–O thin films by reactive magnetron sputtering, J. Mat. Res. Technol. 8 (1) (January – March 2019) 690–696, https://doi.org/10.1016/j.jmrt.2018.05.013.
[34] A. Kosarian, M. Shakiba, E. Farshidi, Role of sputtering power on the microstructural and electro-optical properties of ITO thin films deposited using DC sputtering technique, IEEJ T Electr. Electr. 13 (1) (September 2017), https://doi.org/10.1002/tee.22494.
[35] M.P. Taylor, D.W. Readey, M.F.A.M. van Hest, C.W. Teplin, J.L. Alleman, M. S. Dabney, L.M. Gedvilas, B.M. Keyes, B. To, J.D. Perkins, D.S. Ginley, The remarkable thermal stability of amorphous in-Zn-O transparent conductors, Adv. Funct. Mater. 18 (20) (October 2008) 3169–3178, https://doi.org/10.1002/adfm.200700604.
[36] E. Alfonso, J. Olaya, G.I. Cubillos, Thin Film Growth through Sputtering Technique and its Applications, Chapter book, Crystallization-Science and Technology, September 2012, https://doi.org/10.5772/35844.
[37] Y.J. Kim, S.B. Jin, S.I. Kim, Y.S. Choi, I.S. Choi, J.G. Han, Study on the electrical properties of ITO films deposited by facing target sputter deposition, 42, March 2009, https://doi.org/10.1088/0022-3727/42/7/075412, 075412 (5 pages).
[38] J.R. Bellingham, W.A. Phillips, C.J. Adkins, J. Phys.:Condes. Matter 2 (1990) 6201.
[39] A.H. Sofi, M.A. Shah, K. Asokan, Structural, optical and electrical properties of ITO thin films, J. Electron. Mater. 47 (2) (February 2018) 1344–1352, https://doi.org/10.1007/s11664-017-5915-9.
[40] K. Aijo John, V. Kumar, M. Deepak, T. Manju, Influence of sputtering power on the optical properties of ITO thin films, AIP Conf. Proc. 1620 (February 2015) 22, https://doi.org/10.1063/1.4898214.
[41] A.P. Amalathas, M.M. Alkaisi, Effects of film thickness and sputtering power on properties of ITO thin films deposited by RF magnetron sputtering without oxygen, J. Mater. Sci. Mater. Electron. 27 (May 2016) 11064–11071, https://doi.org/10.1007/s10854-016-5223-9.
[42] A.V. Mudryi, A.V. Ivaniukovich, A.G. Ulyashin, Deposition by magnetron sputtering and characterization of indium tin oxide thin films, Thin Solid Films 515 (February 2007) 6489–6492, https://doi.org/10.1016/j.tsf.2006.11.113.
[43] M. Higuchi, S. Uekusa, R. Nakano, K. Yokowaga, Postdeposition annealing influence on sputtered indium tin oxide film characteristics, Jpn. J. Appl. Phys. 33 (January 1994) 302–306, https://doi.org/10.1143/jjap.33.302.
[44] L. Kerkachea, A. Layadi, A. Mosser, Effect of oxygen partial pressure on the structural and optical properties of dc sputtered ITO thin films, J. Alloys Compd. 485 (June 2009) 46–50, https://doi.org/10.1016/j.jallcom.2009.06.103.
[45] J. Haschke, O. Dupré, M. Boccard, C. Ballif, Silicon heterojunction solar cells: recent technological development and practical aspects - from lab to industry, Sol. Energy Mater. Sol. Cells 187 (2018) 140–153.
[46] S. Walheim, E. Schaffer, J. Mlynek, U. Steiner, Nanophase-separated polymer films as high-performance antireflection coatings, Science 283 (January 1999) 520–522, https://doi.org/10.1126/science.283.5401.520.
[47] D. Poitras, J.A. Dobrowolski, Toward perfect antireflection coatings. 2. theory, Appl. Opt. 43 (2004) 1286–1295, https://doi.org/10.1364/AO.43.001286.